# Fabrication of Fluorescent PMMA-Carbon Nanodots Optical Films and their Feasibility in Improving Solar Cells Efficiency using Low-Cost Sustainable Materials

Marco César Prado Soares ( ✉ marcosoares.feq@gmail.com )

State University of Campinas: Universidade Estadual de Campinas   https://orcid.org/0000-0002-5219-5124

**Michele Cacioppo**

University of Trieste: Universita degli Studi di Trieste

**Francesco Amato**

University of Trieste: Universita degli Studi di Trieste

**Thiago D. Cabral**

State University of Campinas: Universidade Estadual de Campinas

**Marcelo N. P. Carreño**

University of Sao Paulo: Universidade de Sao Paulo

**Inés Pereyra**

University of Sao Paulo: Universidade de Sao Paulo

**Carlos A. S. Ramos**

University of Sao Paulo: Universidade de Sao Paulo

**Manuel Cid**

University of Sao Paulo: Universidade de Sao Paulo

**Gilson S. Goveia**

University of Sao Paulo: Universidade de Sao Paulo

**José F. D. Chubaci**

University of Sao Paulo: Universidade de Sao Paulo

**Eric Fujiwara**

State University of Campinas: Universidade Estadual de Campinas

**Julio R. Bartoli**

State University of Campinas: Universidade Estadual de Campinas

**Research Article**

---

# Abstract

Nitrogen-doped carbon nanodots synthesized from L-arginine and ethylenediamine (NCNDs); citric acid-derived carbon nanodots with carboxylic surface groups (α-CDs); and Silica-Cdots hybrids produced through coupling α-CDs to $SiO_2$ nanoparticles were used for the fabrication of fluorescent PMMA-CDs optical films. PMMA naturally emits luminescence when irradiated by 300-320 nm and the nanoparticles occlusion allows the conversion of a broader UV bandwidth to the visible: emissions around 450 nm are observed for excitations from 330-360 nm. Since this photoluminescence could increase the efficiency of solar energy concentrators and generators, photovoltaic cells were coated with films obtained with the blue-emitting NCNDs for a proof-of-concept of increasing the cells' efficiencies with such materials. At our preliminary experiments, even using a setup with low contact of the optical polymer film on silicon surface, a promising increase from 4.24% to 4.72% cell efficiency was observed, showing the feasibility and potential for application of these environmentally friendly materials.

# 1. Introduction

Carbon Nanodots (CDs) are fluorescent nanoparticles characterized by various surface functional groups and sizes below 10 nm [1, 2]. The conversion of organic precursors containing carboxylic acids (or nitrogen as doping element) results in the formation of CDs rich in carboxylic (or amine) surface groups with enhanced luminescence [3].

Beyond the low-cost, CDs are environmentally safe materials [3, 4] with good biological and biocompatibility properties, being excreted in urine [1, 5]. Their fluorescence finds applications as light converters for photovoltaic cells with improved efficiency and may replace dye sensitizers [6, 7]. Besides, CDs show a plethora of applications, from imaging and sensing to the fabrication of high-tech optoelectronic devices, like white-light or color-modulated LEDs [3, 6]. They can be also combined to polymeric materials [8–10]: interesting polymeric nanocomposites may be obtained through several techniques like *in-situ* polymerization, reticulation, and solution or melt blending. When nanoparticles dimensions are within the molecular levels of polymer chains, such nanocomposites may exhibit enhanced properties derived from the combination of the materials [11, 12].

For optical applications, in turns, the use of poly (methyl methacrylate), PMMA, is particularly interesting for the design of nanocomposite matrices. PMMA is a highly transparent thermoplastic and an amorphous polymer in an intermediate position between commodities and engineering thermoplastics. So, it presents relative low cost and good mechanical strength, combining fracture resistance to optical transmittance [13, 14]. Thus, PMMA-CDs composites with fluorescence properties have potential applications in Light-Emitting Devices (LEDs) [15], Luminescent Solar Concentrators (LSCs) [16], Dye-Sensitized Solar Cells (DSCs) [17] and Organic Solar Cells (OSCs) [1, 18–22]. In such cases, the polymer matrix is not only responsible for the device's mechanical support, but also for the dispersion of the nanodots and prevention of the solid-state quenching [22].

In competition with CDs, organic dyes or inorganic quantum dots have been much more used as PMMA doping substances [23–25]. However, there are some problems with these dopants, either with the stability of organic dyes or with the toxicity of inorganic elements (CdTe, PbSe) [26–30]. In turn, the improvement in the energy conversion efficiency of solar cells can be achieved with LSCs or Luminescent Down Shifting (LDS) devices using low-cost and environmentally friendly fluorescent carbon dots [31–34].

In light of these aspects, this work proposes an approach for the fabrication of PMMA optical films doped with carbon nanodots by solution casting. CDs exhibit a good solubility in polar solvents like methanol, whereas PMMA is very soluble in chloroform. As it was previously defined that 2:1 (v/v) is the best ratio between chloroform and methanol to dissolve CDs, this proportion was applied to the solutions of PMMA and chloroform [35]. So, the nanocomposites optical films were produced by drop-casting PMMA/CDs solutions, and the optical films were doped with three different kinds of CDs for being tested regarding the fluorescent emissions. Finally, solar cells were coated with these nanocomposites in a simple proof-of-concept of the possibility of increasing the energy conversion efficiency.

## 2. Materials and Methods

## 2.1. Nitrogen-doped carbon nanodots synthesis

Blue-emitting nitrogen-doped carbon nanodots (NCNDs) from L-arginine (Fluorochem; ≥98%) and ethylenediamine (EDA, Sigma-Aldrich; ≥99.5%) are obtained through the bottom-up procedure previously described in literature [36].

For that, the two organic precursors at 1:1 (mol/mol) ratio are mixed to ultrapure water (>18 MΩ Milli-Q, Millipore): 87.0 mg of arginine are mixed to 33.0 μL EDA in 100.0 μL Milli-Q water and this solution is introduced into a CEM Discover-SP microwave oven with controlled conditions (240°C, 26 bar and 200 W) for 180 seconds (reaction represented in Fig. 1a). The microwave treatment converts the transparent medium into a brown-colored solution (Fig. 1b), which is then diluted in water and filtered through a 0.1 μm microporous membrane for separating a deep yellow liquid (Fig. 1c). As shown in Fig. 1d, this filtered solution emits a strong blue fluorescence when irradiated at 365 nm ultraviolet (UV) light [37]. Finally, the yellow solution is dialyzed against pure water through a dialysis membrane with molecular weight cut-off of 0.5-1 kDa (Spectrum Labs) for 2 days (water refreshed every 6 hours) [35].

The dialyzed solution of NCNDs is lyophilized using a bench-top freeze-dryer (LaboGene ScanVac CoolSafe; -49°C; 72 h of vacuum). Each synthesis results in ca. 23.0 mg of a brownish solid, so 11 batches are run to obtain 250 mg of NCNDs. It is demonstrated that this procedure is quite reproducible, and previous characterizations reveal that the obtained fluorescent NCNDs present relative quantum yield (QY) of 0.17 [36]; narrow distribution of diameters (1.0-4.5 nm); and plenty of surface traps and functional groups that allow tuning the luminescent emissions. The NCNDs fluorescence shows a broad

emission peak at 356 nm when excited at 300 nm and a bathochromic shift from 356 to 474 nm as the excitation changes from 300 to 420 nm [37, 38].

## 2.2. α-CDs and Silica-Cdots hybrids production

Citric acid-derived carbon nanodots (α-CDs) and the nanocomposites formed by combining them with $SiO_2$ nanoparticles (Silica-Cdots) are used as produced and characterized in a previous report [9].

Briefly, α-CDs with sizes from 4 to 10 nm (mostly around 6 nm) are synthetized from the thermolysis of citric acid (200 g, Fluka, 99.5%) in a muffle furnace under air atmosphere at 180°C for 40 h. In turns, commercial fumed silica nanoparticles (206 mg Aerosil 300, primary particle size ca. 7 nm, Evonik) are dispersed in ethanol (5 mL) and treated with 3-aminopropyltriethoxysilane (APTES, 5 mL). This dispersion is stirred overnight at room temperature (r.t.) before being purified by centrifugation; dispersed in ethanol (three times); and lyophilized for obtaining amino-functionalized silica nanoparticles (a-$SiO_2$).

Finally, a-$SiO_2$ (50 mg) is mixed to the α-CDs (223 mg) dispersed in dimethylformamide (DMF, 10 mL) in the presence of 1-ethyl-3-(3-dimethylaminopropyl) carbodiimide hydrochloride (200 mg, EDC•HCl Alfa Aesar) and N-hydroxysuccinimide (120 mg NHS, Sigma Aldrich). This mixture is stirred at 70°C for 2 days, and DMF is removed through azeotropic distillation with toluene. Milli-Q water is added, and the system is purified by centrifugation (two cycles of 20 min at 3000 rpm) for obtaining Silica-Cdots nanohybrids with sizes on the order of 50 nm, nitrogen and oxygenated surface groups, and excitation-dependent fluorescence. The maximum intensity is observed for the 360 nm-excitation (emission at 465 nm), and the emission shifts from 465 to 513 nm (green) as the excitation changes from 360 to 430 nm [9].

## 2.3. Preparation of doped-PMMA optical films

The synthesized carbon nanodots are used to prepare nanocomposites with PMMA by solution blending: PMMA pellets are dissolved in chloroform, whereas previously lyophilized nanodots are dispersed in a solution of methanol and chloroform. The solutions are mixed, and thin films of nanocomposites are finally prepared by drop-casting on a glass substrate (Petri dishes).

PMMA pellets (Plexiglas V0 52, Arkema) are previously dried in an oven for 4 h at 80 °C and left cool down to room temperature in a vacuum chamber with drier agent. For the preparation of a PMMA optical film by casting, a ratio of 21.5:1 (mL/g) of chloroform and PMMA is used. For instance, an optical film with diameter of 50 mm and thickness of ~ 100 μm is obtained with 232 mg of PMMA. Then, 5 mL of chloroform (Sigma-Aldrich) are added to the PMMA pellets, and the system is left under magnetic stirring for 2 h at room temperature, followed by 20 s of ultrasound bath treatment.

Lyophilized carbon nanodots are dispersed in a mixture of chloroform and methanol, 2:1 (v/v) according to the best ratio previously defined [35] and subsequently kept in an ultrasound bath for 10 min. One example of dispersion prepared with this procedure is shown on Figure SI 1 (Supporting Information), where α-CDs (5 wt%) are observed under daylight and under 365 nm UV light.

After that, a CDs dispersion is simply added to that of PMMA-chloroform and mixed in an ultrasound bath for more 10 min. Different CDs-PMMA systems are prepared according to the desired concentration of CDs, from 0.1–5% in mass (for instance, Figure SI 2 (Supporting Information) shows the aspect of the solution obtained for the system PMMA-NCNDs (5 wt%)).

Next, the optical films are produced by solution casting onto Petri dishes, slowly pouring (drop-by-drop) the CDs-PMMA solution with a pipette. For this step, the dishes must already be leveled to evenly maintain the thickness of the casted volume (a leveling instrument is used). Finally, the Petri dishes are left to dry in atmosphere saturated with chloroform vapor (room temperature) for 48–72 h to avoid formation of microvoids due to rapid volatilization. The saturated atmosphere is created by placing several vials containing chloroform close to the Petri dishes, keeping the set covered to ensure isolation from the room. A PMMA casting film with no carbon nanodots (pristine sample) is also prepared through this same procedure. The optical films formed on the Petri dishes are weighed after 24 h, 48 h and 72 h, until the mass losses due to the evaporation of chloroform are stabilized. Figure SI 3 (Supporting Information) shows the aspect and the blue fluorescence observed (λ = 365 nm irradiation) from a PMMA-NCNDs (5 wt%) film formed on the Petri dish.

## 2.4. Films' fluorescence and photovoltaic characterizations

The PMMA-CDs film is cut from the bottom of the Petri dish (with a scalpel) in the shape of a 45 mm × 13.5 mm rectangle. Then, the dish is taken to the freezer for 1 to 2 min to allow the polymeric film to lose contact with its bottom. After that, a spatula may be used to remove the film, which must have its mass and thickness assessed before the fluorescence evaluation. Figure 2 shows the aspect of one film formed with PMMA and NCNDs (0.5 wt%) when the material is observed under daylight and under 365 nm-UV light.

So, PMMA films had their photoluminescence (PL) spectra analyzed at room temperature with a Cary Ellipse-Varian Fluorescence Spectrophotometer (Agilent Technologies) at excitation wavelengths from 300 to 360 nm, 600 nm/min scan speed, and excitation and emission slits of 5 nm. For that, quartz cuvettes (High Precision Cell Suprasil, light path 10 × 10 mm, Hellma Analytics) were adapted for solid analysis, allowing rectangular films to be inserted into the cuvettes' diagonal positions (13.5 mm). Since the films are thin and flexible, they may show a curvature after their insertion into a cuvette. Thus, it is necessary to verify if the modification of the curvature direction (concave or convex) has any effect on the PL spectra for a given film. A Fluorolog 3 Fluorescence Spectrophotometer (Horiba) equipped with solid sample holders for thin films was also used in the characterization of the very thin optical films produced.

Photovoltaic measurements were performed with home-made silicon-based solar cells (laboratory scale, usually destined to didactic purposes) with dimensions of 25 mm × 25 mm and maximum efficiency of 5%. The tests were conducted by simply positioning and holding the pristine PMMA and doped PMMA-CDs optical films on the external surfaces of the solar cells.

The solar cells were tested on a bench designed for photovoltaic measurements [39]. This bench is equipped with a solar simulator where the light source is a xenon power supply XPS 300 (Solar Light) adjusted for an incident intensity of 1000 W/m$^2$ equivalent to AM 1.5 solar irradiance. A thermostatic bath keeps the test temperature constant at 25 ºC, and the I × V curves of the photovoltaic devices are measured with a digital multimeter HP 34401A (Hewlett Packard) and the Lab Tracer 2.0 (Keithley) software. Also, the measurement system uses a standard solar cell with short-circuit current $I_{sc}$ = 66.40 mA. The solar cells and the testing bench are shown on Figure SI 4 (Supporting Information).

# 3. Results and Discussion

## 3.1. Films fluorescence emission study

The bare PMMA film shows a natural fluorescence emission when irradiated from 300−320 nm (broad emission peak around 450 nm), but there is no luminescence for irradiations at longer wavelengths (Fig. 3a). If compared to the pristine material, the PMMA-NCNDs films reveals additional emission bands for excitations longer than 320 nm (Figs. 3b-d).

From the films produced using chloroform/methanol 2:1, it is possible to discern the PMMA typical bands (without shifts) and the CDs ones with low intensity. The lower intensity of CDs emissions could be related to: (*i*) the low number of light emitters in the matrix [8, 33, 40, 41]; (*ii*) the fluorescence quantum yield of the emitters (also related to the type of carbon dots used) [41]; (*iii*) the matrix-related effects and the quality of nanoparticles dispersion (which could be correlated to the quenching or modification of the emissive domains on each dot) [40]; and (*iv*) solvatochromic effects [42−44]. In addition, quenching phenomena could occur, as carbon dots can act as electron donors or acceptors in their excited states [45, 46].

As support to the previous expectations, the composition of the solvent mixture is quite important on modulating the fluorescence emission of the film (Figs. 3c-d). In particular, the matrices obtained for chloroform/methanol ratios of 3.3:1 and 4:1 still show the PMMA emissions, but there are broader NCNDs emission bands with undistinguishable maximum (~ 400−450 nm). From these data, the solvent mixture ratio 2:1 resulted in the best compromise in terms of NCNDs emission for the study prosecution.

To test the hypotheses that the intensities verified could be related to the concentration or to the intrinsic nature of the occluded carbon nanodots, higher concentrations of NCNDs (5 wt%) were tested and compared against the same concentrations of other two particles (α-CDs and Silica-Cdots). A PMMA-α-CDs solution used on this experiment (before casting) is shown on Figure SI 5 (Supporting Information), whereas the PL results are present in Fig. 4. The increase on the NCNDs nanoparticles concentration resulted in more defined and intense emission bands for the dots emissions, slightly higher than the PMMA matrix. Now, the maxima for emissions from 330−360 nm are clearly centered at ca. 450 nm. Thus, the contribution of nanoparticles in PMMA-NCNDs films extends the range of intense fluorescence emissions for excitations up to 360 nm.

Interestingly, a superior behavior was obtained when testing the other two nanoparticles (α-CDs and Silica-Cdots hybrids), with several emission peaks showing higher intensities than the emissions from the matrix. The peaks are still centered in ca. 450 nm, and Fig. 4b (α-CDs) presents all CDs emissions above the PMMA's (peaks increasing with the excitation wavelength). Also, emissions observed for 350 and 360 nm overcame 1000 a.u. (arbitrary units) and saturated the detector, so they were omitted from Fig. 4b.

Lastly, Fig. 4c shows lower intensities for the hybrids when their spectra are compared to the α-CDs (some hybrids' bands present less intensity than the PMMA ones). This is probably related to the very larger dimensions of the hybrids and to the modification of the surface functional groups due to the coupling reaction between the α-CDs carboxylic acids and the $SiO_2$ nanoparticles (which removes some of the free -COOH). Such structural differences modify the interactions between the dispersed phase and the acrylate matrix. Also, these differences can add new changes to the quenching mechanisms or to the emissive domains on each nanodot [9, 40, 43, 47].

The saturation observed on Fig. 4b suggests that the modification of the equipment's operational parameters and the analysis of longer excitation wavelengths could show better results and even reveal the presence of other relevant emission bands for these dots. So, the analysis was repeated, but the excitation and emission slits were reduced from 5 to 2.5 nm.

As shown on Figure SI 6 (Supporting Information), the slits reduction results in spectra which much lower intensities: as a matter of fact, only the PMMA-α-CDs system could be analyzed, since the intensities observed for the other two materials were too low to result in sufficiently resolved peaks adequate for the comparison between curves and composites. The new spectra show no saturation; intensities increasing with excitations from 340 to 370 nm; and a clear emission maximum at 425 nm, corresponding to the excitation at 370 nm. This increase of the intensity with the excitation wavelength was not observed on other systems, as noticeable in Fig. 4.

The films observed under daylight and under UV radiation (λ = 365 nm) are shown in Figure SI 7 (Supporting Information). Their absorption and transmittance properties, in turn (obtained with the spectrophotometer), are compared in Figures SI 8–9 (Supporting Information).

In Figure SI 8, the UV-Visible absorption spectra for the nanodots composites show maximum absorbance at 250 nm, corresponding to the $\pi \to \pi^*$ transition of the $sp^2$ carbons of the CDs cores; and shoulders at 275–300 nm with tails extending to the visible range, assigned to the $n \to \pi^*$ transitions involving the electron lone pairs of the carboxylic and nitrogen surface groups [8, 9]. The pristine presents almost no absorbance on the analyzed range, whereas the PMMA-α-CDs is the composite with highest capability on absorbing the ultraviolet. This behavior is approximately opposite to the observed for the transmittances (Figure SI 9): until 300 nm, pristine has a transmittance considerably higher than the others; whereas the PMMA-α-CDs shows a slower sigmoidal increase of the transmittance, reaching a value close to 100% only after 500 nm. The Silica-Cdots nanocomposite has the highest transmittance on

the visible, what may be consequence of the high transmittance, capability of conducting light and optical properties observed on silica-based materials [48, 49].

## 3.2. Screening of the photovoltaic properties

Carbon nanodots show interesting applications in photocatalysis and renewable energies and can be used in solar concentrators (LSC) or converter (LDS) devices. These devices are designed to collect solar light by absorbing incident photons and reemitting them through an optical waveguide [1, 15, 20].

In general, the LSC collector is composed of thin plates or sheets of a transparent material doped with luminescent species, so that it allows the diffuse incident sunlight to reach these species; and then permits their visible emissions to reach the waveguide [50–52]. Finally, the waveguide directs the photons to the photovoltaic cells positioned on the substrate's extremity, improving the energy conversion efficiency. In turn, solar converters (LDS) are films or photoluminescent layers deposited and adhered on the surface of solar cells or photodiodes. LDSs have the same function of shifting the solar spectrum to longer wavelengths (down shifting), reducing UV radiation to visible light [32, 53].

Due to its great optic properties, PMMA is one of the most applied materials for manufacturing LSCs [50] and LDSs [32]. In general, these LSCs use organic dyes or inorganic quantum dots as fluorescent species, showing disadvantages such as the photodegradation of the organic dyes or the toxicity of the inorganic nanoparticles [23, 24, 53]. Thus, the photoluminescent behavior of the PMMA-CDs matrices could be exploited to improve the External Quantum Efficiency (EQE) of photovoltaic cells, considering the large-scale systems' production costs [50].

Actually, some carbon nanodots-based composites were already leveraged on solar energy applications [31–33]. PMMA-doped films were used as luminescent solar collectors and cells' top-layers, converting UV to visible light. That is because silicon-based solar cells show poor light harvesting performance under UV-irradiation, leading to poor quantum efficiencies in the UV region [35, 54].

Most of the incident UV photons produce photogenerated carriers (electron-hole pairs) close to the surface, which could easily recombine with defect sites in the depletion region, the intermediary zone of the solar cell's p-n junction where the electric current is generated. Thus, NCNDs could facilitate the down-conversion effect on silicon cells: photons with longer wavelengths (in the visible range) could be absorbed and excite carriers in the depletion region for immediate photogenerated carrier separation due to the built-in electric field, leading to increased photovoltaic effect [32, 35, 54].

Therefore, once PMMA-CDs nanocomposites are promising candidates for solar cells applications, NCNDs-doped optical films were used in preliminary experiments (proof-of-concept) of improvement of cell's efficiency. At this purpose, doped films were simply positioned on the external surfaces of silicon-based solar cells with dimensions of 25 mm × 25 mm.

The photovoltaic results (current I versus voltage V for a given incident irradiance power $P_{in}$) obtained for the cell with pristine sample are compared to the NCNDs-doped (0.5 wt%) optical film ones in Fig. 5, and

the experimental parameters evaluated from these tests are shown in Table 1. Here, the short-circuit current $I_{sc}$ is the current through a solar cell when the system is short-circuited (voltage across the cell is zero), i.e., it is the maximum current that may occur on the cell. This current is due to the generation and collection of light-generated carriers and, for an ideal solar cell at moderate resistive loss mechanisms, it is identical to the light-generated current [55]. The open-circuit voltage $V_{oc}$, in turns, is the maximum voltage available for a solar cell, occurring at zero current. It corresponds to the amount of forward bias on the solar cell due to the bias of the cell junction with the light-generated current [56].

$V_{oc}$ presents a complex non-linear relation with temperature and increases with the bandgap, whereas $I_{sc}$ decreases with this gap. In an ideal device, $V_{oc}$ is limited by radiative recombination (electron-hole) [56]. $I_{sc}$, on the other hand, depends on a series of factors, including: (*i*) the area of the solar cell (the short-circuit current density $J_{sc}$ in mA/cm² is the commonly preferred parameter to avoid dependence with cell's top area); (*ii*) the number of incident photons, which may be understood as the power of the incident light source $P_{in}$ ($I_{sc}$ is directly dependent on the light intensity); (*iii*) the spectrum of the incident light; (*iv*) the optical properties (absorption, transmittance and reflection) of the solar cell; (*v*) and the minority-carrier collection probability of the solar cell, which mainly depends on the surface passivation and on the minority carrier lifetime in the cell's base [55].

For both $I_{sc}$ and $V_{oc}$ conditions, the power of the cell is zero. Then, another parameter called the fill factor (FF) is used in conjunction with them to determine the efficiency of the cell. It is given by the relation between the maximum power $P_{max}$ of the cell and the product between $I_{sc}$ and $V_{oc}$. This relation is defined as Eq. (1) [57].

$$FF = \frac{P_{max}}{(V_{OC} \times I_{SC})} (1)$$

FF may be understood as a measurement of the "*squareness*" of the solar cell's I × V curve and is also the area of the largest rectangle which may be inscribed in this plot. The FF from a solar cell can be determined by differentiating its power with respect to the voltage and finding the maximum $P_{max}$ (point where dP/dV = 0): the rectangle area is obtained by multiplying the V of maximum power by the correspondent current value retrieved from I curve [57]. From these parameters, the efficiency of the solar cell η may be finally calculated as Eq. (2) or, in percent, as Eq. (3) [33].

$$\eta = \frac{(J_{SC} \times V_{OC} \times FF)}{P_{in}} (2)$$

$$\eta = \frac{(J_{SC} \times V_{OC} \times FF)}{P_{in}} \times 100\% (3)$$

The current density $J_{sc}$ is related to the cell's transmission and to the amount of excited photoelectrons in the device, presenting a great influence on the overall efficiency of the system [58]. Moreover, previous

studies with carbon nanodots-doped light solar concentrators indicate that both $J_{sc}$ and $V_{oc}$ should increase with the concentration of nanoparticles. Since the total of excited photoelectrons is associated with the doping concentration, the intensity of the emitted fluorescence increases with CDs concentration. Gong *et al.* (2018) argue that such increase is not indefinitely, though, so the concentration of nanoparticles shows an optimal value. It is a consequence of the fact that there is some overlap between the absorption spectra and the fluorescence emission spectra of carbon nanodots, then the emitted photons may be absorbed by the CDs themselves. Thus, as the doping concentration increases, so does the probability of collision between nanoparticles and photons, what enhances the self-absorption effect. Finally, once the fluorescence quantum efficiency must be smaller than 1 [41], the final emitted fluorescence intensity is necessarily smaller than the absorbed intensity, resulting in a loss of total light intensity. Therefore, if the doping concentration exceeds the optimum value (a condition that must be determined empirically), the fluorescence intensity and the solar cell's efficiency will start decreasing [33].

In Fig. 5 and Table 1, the I × V curve and photovoltaic parameters are presented for a PMMA-0.5 wt% NCNDs and pristine optical films (both with ~ 35 µm thicknesses). An increase in the solar cell efficiency is observed for the NCNDs-doped matrix, from 4.24 to 4.72%. Even though one may consider this improvement (11.3%) of low significance, it could be actually considered a promising result. Such judgement stands because this proof-of-concept experiment has been performed using films doped with CDs nanoparticles with lowest emission intensities (NCNDs) and at low concentration (0.5 wt%). Moreover, it should be considered that the coating area of the polymeric films is of only ¼ of the cell's surface, what reduces the number of light emitters on the total area.

Besides, the setup is based on the simple partial superposition of the optical films on the cell's surfaces, leading to: (*i*) poor interface contact conditions; (*ii*) the possible formation of an intermediate air layer (dielectric); (*iii*) film thickness effects. Light reflections may be observed on a setup like this, as the PMMA layer is not adhered on the cell surface. The reflections naturally reduce the conversion efficiency, since they may direct part of the light back to the external medium and can originate light interference phenomena (like a Fabry-Pérot interferometer). Therefore, the reduction of the film's reflectance could be a strategy for improving the energy conversion [48, 59]. Naturally, the use of the most-efficient carbon nanodots (α-CDs) is also expected to lead to better results, since they present the most intense emissions.

Table 1
Photovoltaic data obtained for the two tested solar cells covered with pristine and PMMA-NCNDs optical films.

|  | Pristine | PMMA-NCNDs |
|---|---|---|
| $I_{sc}$(mA) | 23.87 | 26.55 |
| $V_{oc}$(V) | 0.6069 | 0.6098 |
| $J_{sc}$(mA/cm²) | 9.95 | 11.06 |
| $P_{max}$(mW) | 10.18 | 11.32 |
| FF | 0.703 | 0.699 |
| η (%) | 4.24 | 4.72 |

# 4. Conclusions

Three typologies of carbon dots, namely NCNDs, α-CDs and Silica-Cdots hybrids, were applied to the fabrication of fluorescent PMMA optical films. The PMMA-CDs optical films show broad fluorescence emission centered in 450 nm when irradiated from 300 to 360 nm. The PMMA matrices of the pristine films show the broad fluorescence around 450 nm when excited only under 300-320 nm, and no emissions for longer wavelengths. Thus, the addition of the CDs nanoparticles to the PMMA allows the conversion of a wider UV-window to the visible.

Besides, PMMA-NCNDs optical films had their PL spectra evaluated to establish the suitable ratio 2:1 between chloroform and methanol to be used on their fabrication process. Also, optical films containing 5 wt% of each kind of nanoparticle had their emissions compared.  The α-CDs present the most intense and resolved luminescence bands, with peaks higher than those corresponding to PMMA fluorescence. Even though the optical films with Silica-Cdots hybrids show emissions superior to the ones obtained for NCNDs, they are slightly slower than the α-CDs, what is probably related to their larger dimensions and to the modification of the surface functional carboxylic groups. The spectra of α-CDs showed a degree of saturation for the 360 nm-excitation, so smaller slits were used to observe intensities that increase as excitation goes from 340 to 370 nm, presenting maximum emission at 425 nm (correspondent to 370 nm excitation).

Finally, an optical film of NCNDs-doped PMMA (film with lowest emission intensities) was simply positioned on a solar cell as proof-of-concept of the possibility of using the nanocomposites for improving the efficiency of these photovoltaic devices. Despite the poor contact conditions and of some reflections on PMMA, an increase from 4.24 to 4.72% was observed for the efficiency, showing the feasibility and potential application of these low-cost sustainable materials.

This 11.3% of efficiency gain would be translated into enormous savings of economic and environmental resources on commercial systems. For instance, the photovoltaic cells manufacturers rate their power output using Standard Test Conditions (irradiance of 1000 W/m², spectrum AM 1.5 at 25°C). In such conditions, an average panel presents efficiency of 15%, and a 1 m² surface-panel produces about 150 W [60]. Solar farms are much larger than that, though. According to the National Renewable Energy Laboratory (NREL, USA), the electricity supply for 1000 American houses throughout one year would require a large solar plant capable of generating 1 GWh operating during the whole year. On average, the NREL estimates that 2.8 acres of solar panels are needed for that, corresponding to 32 acres of land for the solar farm [61,62].

Thus, considering that the solar plant has a 15% average efficiency, an increase of 11.3% could bring the efficiency to 16.7%, reducing the total area of the panels to 2.5 acres (10.7% of reduction); and lowering the total land needed for the farm to 28.7 acres (10.3% savings on the required land area).

Upcoming works will use α-CDs (highest PL intensities) as the standard for film fabrication, testing the effects of applying different concentrations of these nanodots. Since these nanoparticles are formed by thermolysis in simple muffles, they are particularly adequate for large-scale manufacturing due to possibility of CDs fabrication using simpler, cheaper, and larger equipment. Also, the very high absorbance observed for these particles on Figure SI 8 indicates that they have the highest capability on protecting the cell against the UV while shifting the radiation to the visible (increasing the convertible window). Moreover, the direct coating of the cells with PMMA could improve the film contact; and eliminate the extra dielectric layer (air) and the successive light reflections. This could be accomplished by drop-casting the PMMA-CDs chloroform solutions directly on the cell's surface; or through spin-coating.

# Declarations

# References

1. Wang Y, Hu A (2014) Carbon quantum dots: synthesis, properties and applications. J Mater Chem C 2:6921. https://doi.org/10.1039/C4TC00988F

2. Kang Z, Lee S-T (2019) Carbon dots: advances in nanocarbon applications. Nanoscale 11:19214–19224. https://doi.org/10.1039/C9NR05647E

3. Đorđević L, Arcudi F, Cacioppo M, Prato M (2022) A multifunctional chemical toolbox to engineer carbon dots for biomedical and energy applications. Nat Nanotechnol 17:112–130. https://doi.org/10.1038/s41565-021-01051-7

4. Boakye-Yiadom KO, Kesse S, Opoku-Damoah Y, Filli MS, Aquib M, Joelle MMB, Farooq MA, Mavlyanova R, Raza F, Bavi R, Wang B (2019) Carbon dots: Applications in bioimaging and theranostics. Int J Pharm 564:308–317. https://doi.org/10.1016/j.ijpharm.2019.04.055

5. Huang X, Zhang F, Zhu L, Choi KY, Guo N, Guo J, Tackett K, Anilkumar P, Liu G, Quan Q, Choi HS, Niu G, Sun Y-P, Lee S, Chen X (2013) Effect of Injection Routes on the Biodistribution, Clearance, and Tumor Uptake of Carbon Dots. ACS Nano 7:5684–5693. https://doi.org/10.1021/nn401911k

6. Wang B, Lu S (2022) The light of carbon dots: From mechanism to applications. Matter 5:110–149. https://doi.org/10.1016/j.matt.2021.10.016

7. Semeniuk M, Yi Z, Poursorkhabi V, Tjong J, Jaffer S, Lu Z-H, Sain M (2019) Future Perspectives and Review on Organic Carbon Dots in Electronic Applications. ACS Nano 13:6224–6255. https://doi.org/10.1021/acsnano.9b00688

8. Perli G, Soares MCP, Cabral TD, Bertuzzi DL, Bartoli JR, Livi S, Duchet-Rumeau J, Cordeiro CMB, Fujiwara E, Ornelas C (2022) Synthesis of Carbon Nanodots from Sugarcane Syrup, and Their Incorporation into a Hydrogel-Based Composite to Fabricate Innovative Fluorescent Microstructured Polymer Optical Fibers. Gels 8:553. https://doi.org/10.3390/gels8090553

9. Amato F, Soares MCP, Cabral TD, Fujiwara E, de Cordeiro CM, Criado A, Prato M, Bartoli JR (2021) Agarose-Based Fluorescent Waveguide with Embedded Silica Nanoparticle–Carbon Nanodot Hybrids for pH Sensing, ACS Appl. Nano Mater 4:9738–9751. https://doi.org/10.1021/acsanm.1c02127

10. Affonso Netto R, de Menezes FF, Maciel Filho R, Bartoli JR (2022) Poly(methyl methacrylate) and silica nanocomposites as new materials for polymeric optical devices, Polímeros. 32 https://doi.org/10.1590/0104-1428.20220009

11. Alexandre M, Dubois P (2000) Polymer-layered silicate nanocomposites: preparation, properties and uses of a new class of materials. Mater Sci Eng R Reports 28:1–63. https://doi.org/10.1016/S0927-796X(00)00012-7

12. Fischer H (2003) Polymer nanocomposites: from fundamental research to specific applications. Mater Sci Eng C 23:763–772. https://doi.org/10.1016/j.msec.2003.09.148

13. Ali U, Karim KJBA, Buang NA (2015) A Review of the Properties and Applications of Poly (Methyl Methacrylate) (PMMA). Polym Rev 55:678–705. https://doi.org/10.1080/15583724.2015.1031377

14. Corsaro C, Neri G, Santoro A, Fazio E (2021) Acrylate and Methacrylate Polymers' Applications: Second Life with Inexpensive and Sustainable Recycling Approaches. Mater (Basel) 15:282. https://doi.org/10.3390/ma15010282

15. Stepanidenko EA, Ushakova EV, Fedorov AV, Rogach AL (2021) Applications of Carbon Dots in Optoelectronics, Nanomaterials. 11 364. https://doi.org/10.3390/nano11020364

16. Ma W, Li W, Liu R, Cao M, Zhao X, Gong X (2019) Carbon dots and AIE molecules for highly efficient tandem luminescent solar concentrators. Chem Commun 55:7486–7489. https://doi.org/10.1039/C9CC02676B

17. Mohan K, Bora A, Dolui SK (2018) Efficient Way of Enhancing the Efficiency of a Quasi-Solid-State Dye-Sensitized Solar Cell by Harvesting the Unused Higher Energy Visible Light Using Carbon Dots, ACS Sustain. Chem Eng 6:10914–10922. https://doi.org/10.1021/acssuschemeng.8b02244

18. Maxim AA, Sadyk SN, Aidarkhanov D, Surya C, Ng A, Hwang Y-H, Atabaev TS, Jumabekov AN (2020) PMMA Thin Film with Embedded Carbon Quantum Dots for Post-Fabrication Improvement of Light Harvesting in Perovskite Solar Cells, Nanomaterials. 10 291. https://doi.org/10.3390/nano10020291

19. Bouknaitir I, Panniello A, Teixeira SS, Kreit L, Corricelli M, Striccoli M, Costa LC, Achour ME (2019) Optical and dielectric properties of PMMA (poly(methyl methacrylate))/carbon dots composites. Polym Compos 40:E1312–E1319. https://doi.org/10.1002/pc.24977

20. Zhao W-S, Li X-X, Zha H, Yang Y-Z, Yan L-P, Luo Q, Liu X-G, Wang H, Ma C-Q, Xu B-S (2022) Controllable Photoelectric Properties of Carbon Dots and Their Application in Organic Solar Cells. Chin J Polym Sci 40:7–20. https://doi.org/10.1007/s10118-021-2637-5

21. Lin X, Yang Y, Nian L, Su H, Ou J, Yuan Z, Xie F, Hong W, Yu D, Zhang M, Ma Y, Chen X (2016) Interfacial modification layers based on carbon dots for efficient inverted polymer solar cells exceeding 10% power conversion efficiency. Nano Energy 26:216–223. https://doi.org/10.1016/j.nanoen.2016.05.011

22. Kwon W, Do S, Lee J, Hwang S, Kim JK, Rhee S-W (2013) Chem Mater 25:1893–1899. https://doi.org/10.1021/cm400517g. Freestanding Luminescent Films of Nitrogen-Rich Carbon Nanodots toward Large-Scale Phosphor-Based White-Light-Emitting Devices

23. Zhou W, Wang M-C, Zhao X (2015) Poly(methyl methacrylate) (PMMA) doped with DCJTB for luminescent solar concentrator applications. Sol Energy 115:569–576. https://doi.org/10.1016/j.solener.2015.03.012

24. Waldron DL, Preske A, Zawodny JM, Krauss TD, Gupta MC (2017) PbSe quantum dot based luminescent solar concentrators. Nanotechnology 28:095205. https://doi.org/10.1088/1361-6528/aa577f

25. Huang K, Liu J, Yuan J, Zhao W, Zhao K, Zhou Z (2023) Perovskite-quantum dot hybrid solar cells: a multi-win strategy for high performance and stability. J Mater Chem A 11:4487–4509. https://doi.org/10.1039/D2TA09434G

26. Moon H, Lee C, Lee W, Kim J, Chae H (2019) Stability of Quantum Dots, Quantum Dot Films, and Quantum Dot Light-Emitting Diodes for Display Applications. Adv Mater 31:1804294. https://doi.org/10.1002/adma.201804294

27. Albaladejo-Siguan M, Baird EC, Becker-Koch D, Li Y, Rogach AL, Vaynzof Y (2021) Stability of Quantum Dot Solar Cells: A Matter of (Life)Time. Adv Energy Mater 11:2003457. https://doi.org/10.1002/aenm.202003457

28. Manshian BB, Jiménez J, Himmelreich U, Soenen SJ (2017) Personalized medicine and follow-up of therapeutic delivery through exploitation of quantum dot toxicity. Biomaterials 127:1–12. https://doi.org/10.1016/j.biomaterials.2017.02.039

29. Bottrill M, Green M (2011) Some aspects of quantum dot toxicity. Chem Commun 47:7039. https://doi.org/10.1039/c1cc10692a

30. Wu T, Tang M (2014) Toxicity of quantum dots on respiratory system. Inhal Toxicol 26:128–139. https://doi.org/10.3109/08958378.2013.871762

31. Li Y, Miao P, Zhou W, Gong X, Zhao X (2017) N-doped carbon-dots for luminescent solar concentrators. J Mater Chem A 5:21452–21459. https://doi.org/10.1039/C7TA05220K

32. Choi Y, Jo S, Chae A, Kim YK, Park JE, Lim D, Park SY (2017) Simple Microwave-Assisted Synthesis of Amphiphilic Carbon Quantum Dots from A 3 /B 2 Polyamidation Monomer Set. ACS Appl Mater Interfaces 9:27883–27893. https://doi.org/10.1021/acsami.7b06066

33. Gong X, Ma W, Li Y, Zhong L, Li W, Zhao X (2018) Fabrication of high-performance luminescent solar concentrators using N-doped carbon dots/PMMA mixed matrix slab. Org Electron 63:237–243. https://doi.org/10.1016/j.orgel.2018.09.028

34. Zhao H (2019) Refractive index dependent optical property of carbon dots integrated luminescent solar concentrators. J Lumin 211:150–156. https://doi.org/10.1016/j.jlumin.2019.03.039

35. Amato F, Cacioppo M, Arcudi F, Prato M, Mituo M, Fernandes EG, Carreño MNP, Pereyra I, Bartoli JR (2019) Nitrogen-Doped Carbon Nanodots/PMMA Nanocomposites for Solar Cells Applications. Chem Eng Trans 74:1105–1110. https://doi.org/10.3303/CET1974185

36. Arcudi F, Đorđević L, Prato M (2016) Synthesis, Separation, and Characterization of Small and Highly Fluorescent Nitrogen-Doped Carbon NanoDots, Angew. Chemie Int Ed 55:2107–2112. https://doi.org/10.1002/ange.201510158

37. Đorđević L, Arcudi F, Prato M (2019) Preparation, functionalization and characterization of engineered carbon nanodots. Nat Protoc 14:2931–2953. https://doi.org/10.1038/s41596-019-0207-x

38. Arcudi F, Đorđević L, Prato M (2017) Rationally Designed Carbon Nanodots towards Pure White-Light Emission, Angew. Chemie Int Ed 56:4170–4173. https://doi.org/10.1002/anie.201612160

39. Stem N (2007) Células solares de silício de alto rendimento: otimizações teóricas e implementações experimentais utilizando processos de baixo custo. Universidade de São Paulo.

https://doi.org/10.11606/T.3.2007.tde-02042008-113959

40. Jiang K, Wang Y, Li Z, Lin H (2020) Afterglow of carbon dots: mechanism, strategy and applications. Mater Chem Front 4:386–399. https://doi.org/10.1039/C9QM00578A

41. Lakowicz JR (2006) Principles of fluorescence spectroscopy, Third. Springer US, Boston, MA. https://doi.org/10.1007/978-0-387-46312-4

42. Chandra S, Singh VK, Yadav PK, Bano D, Kumar V, Pandey VK, Talat M, Hasan SH (2019) Mustard seeds derived fluorescent carbon quantum dots and their peroxidase-like activity for colorimetric detection of H 2 O 2 and ascorbic acid in a real sample. Anal Chim Acta 1054:145–156. https://doi.org/10.1016/j.aca.2018.12.024

43. Bano D, Kumar V, Singh VK, Chandra S, Singh DK, Yadav PK, Talat M, Hasan SH (2019) A Facile and Simple Strategy for the Synthesis of Label Free Carbon Quantum Dots from the latex of Euphorbia milii and Its Peroxidase-Mimic Activity for the Naked Eye Detection of Glutathione in a Human Blood Serum, ACS Sustain. Chem Eng 7:1923–1932. https://doi.org/10.1021/acssuschemeng.8b04067

44. Reichardt C (2005) Polarity of ionic liquids determined empirically by means of solvatochromic pyridinium N-phenolate betaine dyes. Green Chem 7:339–351. https://doi.org/10.1039/b500106b

45. Đorđević L, Haines P, Cacioppo M, Arcudi F, Scharl T, Cadranel A, Guldi DM, Prato M (2020) Synthesis and excited state processes of arrays containing amine-rich carbon dots and unsymmetrical rylene diimides. Mater Chem Front 4:3640–3648. https://doi.org/10.1039/D0QM00407C

46. Cacioppo M, Scharl T, Đorđević L, Cadranel A, Arcudi F, Guldi DM, Prato M (2020) Symmetry-Breaking Charge-Transfer Chromophore Interactions Supported by Carbon Nanodots, Angew. Chemie - Int Ed 59:12779–12784. https://doi.org/10.1002/anie.202004638

47. Cadranel A, Strauss V, Margraf JT, Winterfeld KA, Vogl C, Đorđević L, Arcudi F, Hoelzel H, Jux N, Prato M, Guldi DM (2018) Screening Supramolecular Interactions between Carbon Nanodots and Porphyrins. J Am Chem Soc 140:904–907. https://doi.org/10.1021/jacs.7b12434

48. Saleh BEA, Teich MC (1991) Fundamentals of Photonics. John Wiley & Sons, Inc., New York, USA. https://doi.org/10.1002/0471213748

49. Santos JS, Ono E, Fujiwara E, Manfrim TP, Suzuki CK (2011) Control of optical properties of silica glass synthesized by VAD method for photonic components. Opt Mater (Amst) 33:1879–1883. https://doi.org/10.1016/j.optmat.2011.03.007

50. Reisfeld R, Eyal M, Chernyak V, Zusman R (1988) Luminescent solar concentrators based on thin films of polymethylmethacrylate on a polymethylmethacrylate support. Sol Energy Mater 17:439–455. https://doi.org/10.1016/0165-1633(88)90004-4

51. Barik P, Pradhan M (2021) Plasmonic luminescent solar concentrator. Sol Energy 216:61–74. https://doi.org/10.1016/j.solener.2021.01.018

52. Liu G, Mazzaro R, Sun C, Zhang Y, Wang Y, Zhao H, Han G, Vomiero A (2020) Role of refractive index in highly efficient laminated luminescent solar concentrators. Nano Energy 70:104470. https://doi.org/10.1016/j.nanoen.2020.104470

53. Ahmed H, Kennedy M, Confrey T, Doran J, McCormack SJ, Galindo S, Sánchez CV, González JP (2012) Lumogen Violet Dye as Luminescent Down-Shifting Layer for c-Silicon Solar Cells, in: 27th Eur. Photovolt. Sol. Energy Conf. Exhib., : pp. 311–313. https://doi.org/10.4229/27thEUPVSEC2012-1BV.7.20

54. Tsai M-L, Tu W-C, Tang L, Wei T-C, Wei W-R, Lau SP, Chen L-J, He J-H (2016) Efficiency Enhancement of Silicon Heterojunction Solar Cells via Photon Management Using Graphene Quantum Dot as Downconverters. Nano Lett 16:309–313. https://doi.org/10.1021/acs.nanolett.5b03814

55. Honsberg CB, Bowden SG, Current S-C (2019) Photovoltaics Educ. Website. https://www.pveducation.org/pvcdrom/solar-cell-operation/short-circuit-current (accessed January 24, 2023)

56. Honsberg CB, Bowden SG, Voltage O-C (2019) Photovoltaics Educ. Website. https://www.pveducation.org/pvcdrom/solar-cell-operation/open-circuit-voltage (accessed January 24, 2023)

57. Honsberg CB, Bowden SG, Factor F (2019) Photovoltaics Educ. Website. https://www.pveducation.org/pvcdrom/solar-cell-operation/fill-factor (accessed January 24, 2023)

58. Chung I, Lee B, He J, Chang RPH, Kanatzidis MG (2012) All-solid-state dye-sensitized solar cells with high efficiency. Nature 485:486–489. https://doi.org/10.1038/nature11067

59. Taylor HF (2002) Fiber Optic Sensors Based upon the Fabry-Perot Interferometer. In: Yu FTS, Yin S (eds) Fiber Opt. Sensors, Marcel Dekker,

60. Vourvoulias A, Panels S (2023) GreenMatch. https://www.greenmatch.co.uk/blog/2014/11/how-efficient-are-solar-panels (accessed March 12, 2023)

61. Business S (2013) How Much Land Does it Take to Produce Solar Energy for 1000 Homes?, https://www.sustainablebusiness.com/2013/08/how-much-land-does-it-take-to-produce-solar-energy-for-1000-homes-51784/ (accessed March 12, 2023)

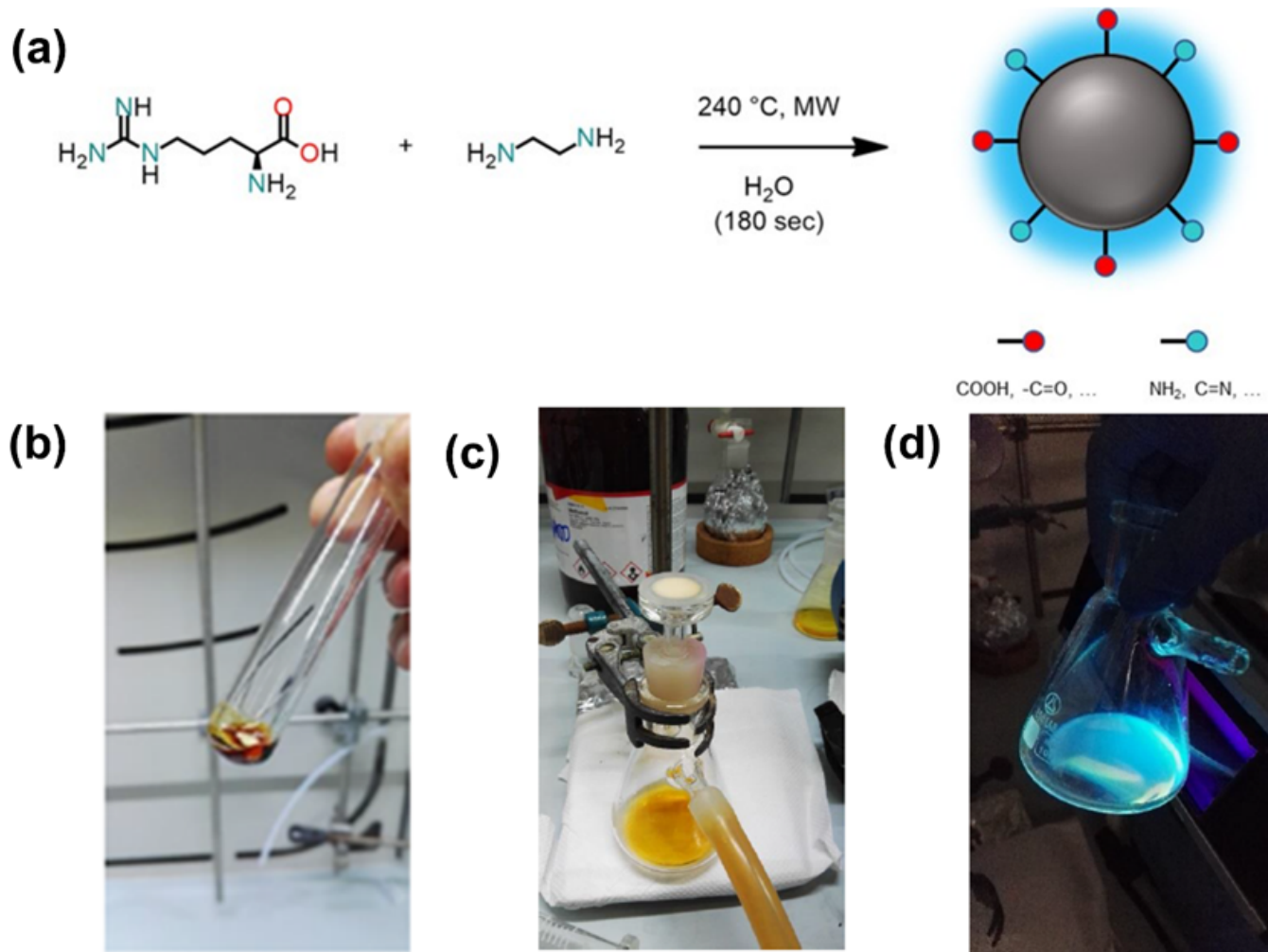62. Ong S, Campbell C, Denholm P, Margolis R, Heath G Land-Use Requirements for Solar Power Plants in the United States, 2013. https://www.nrel.gov/docs/fy13osti/56290.pdf

# Figures

**Figure 1**

a. Scheme of formation of blue-emitting NCNDs; b. brown-colored solution obtained after microwave-assisted synthesis; c. yellow solution obtained after filtering; and d. emission of blue fluorescence by the filtered solution when it is irradiated at 365 nm UV light [35].
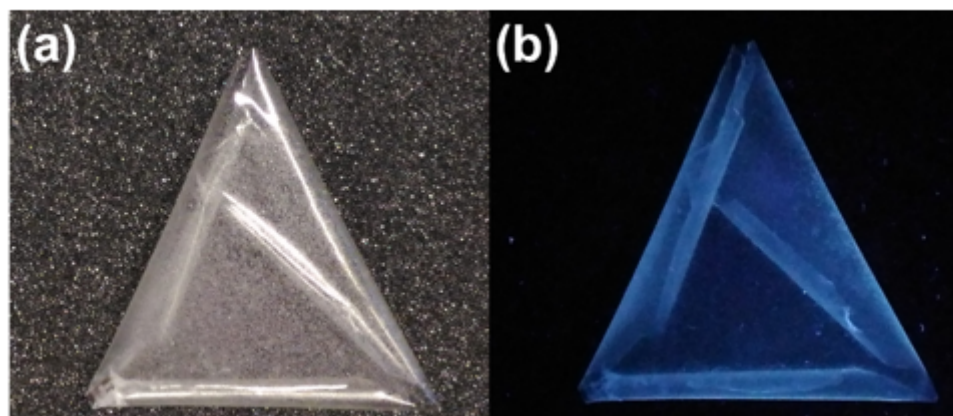


**Figure 2**

PMMA-NCNDs films (0.5 wt%) observed under: **a**. daylight; **b**. UV light (λ = 365 nm).
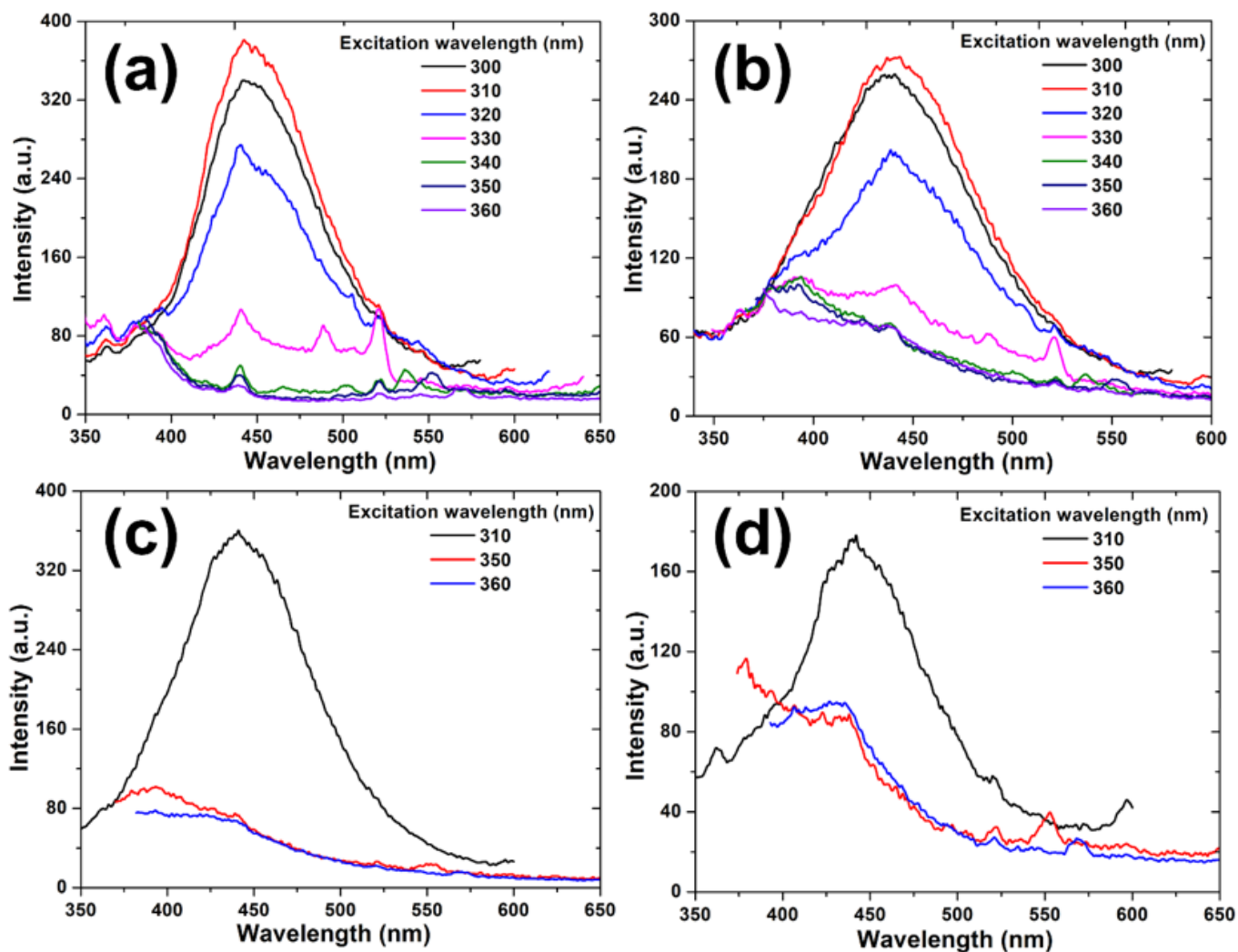


## Figure 3

PL spectra: **a**. PMMA pristine film; and different volumetric proportions of chloroform to methanol for producing PMMA-NCNDs composites (0.1 wt% of CDs). Proportions of: **b**. 2:1 (selected as standard); **c**. (3.3):1; and **d**. 4:1 (v/v).
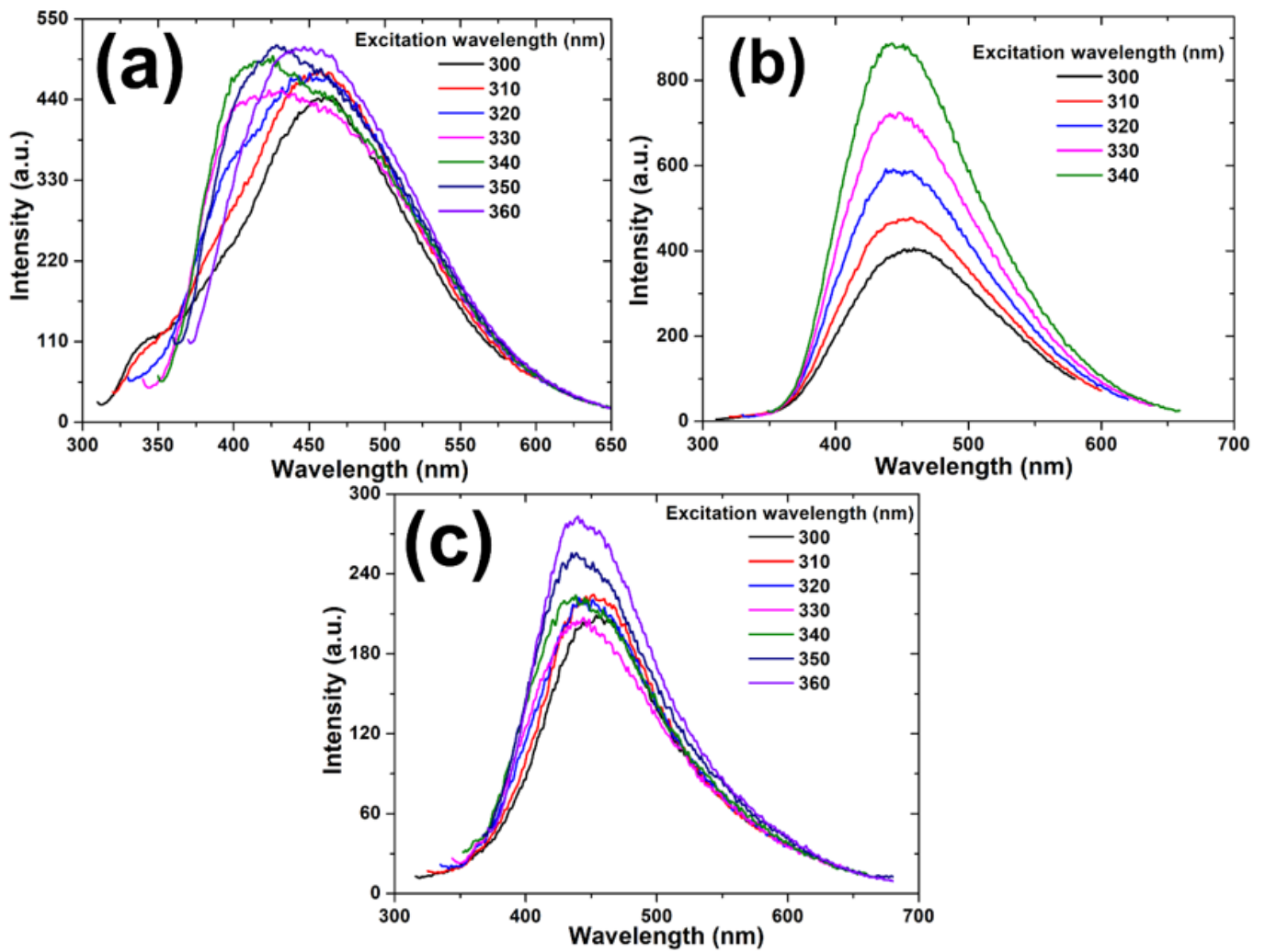
**Figure 4**

PL spectra of films produced by doping PMMA with different amounts of nanoparticles (concentration in mass): **a**. 5 wt% of NCNDs; **b**. 5 wt% of α-CDs (emissions for 350 and 360 nm were omitted, since intensities overcame 1000 a.u. and saturated the detector); and **c**. 5 wt% of Silica-Cdots hybrids.
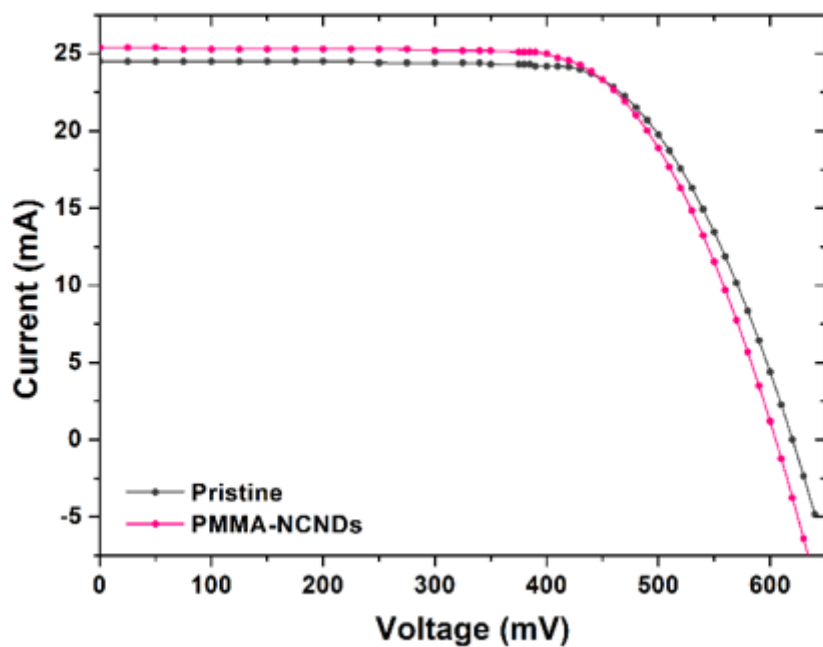
**Figure 5**

Curves of current versus voltage for the solar cells with: (blue) pristine sample; and (red) PMMA-NCNDs optical film.

## Supplementary Files

This is a list of supplementary files associated with this preprint. Click to download.

- GraphicalAbstract.png
- PMMACDfilmsSI.docx